Implication for Using Heme Methyl Hyperfine Shifts as Indicators of Heme Seating as Related to Stereoselectivity in the Catabolism of Heme by Heme Oxygenase: In-Plane Heme versus Axial His Rotation†

Hiroshi Ogura,‡ John P. Evans,§ Paul R. Ortiz de Montellano,§ and Gerd N. La Mar*,‡

Department of Chemistry, University of California, Davis, California 95616, and Department of Pharmaceutical Chemistry, University of California, 600 16th Street, San Francisco, California 94143-2280

Received August 24, 2007; Revised Manuscript Received November 6, 2007

ABSTRACT: The triple mutant of the solubilized, 265-residue construct of human heme oxygenase, K18E/E29K/R183E-hHO, has been shown to redirect the exclusive α-regioselectivity of wild-type hHO to primarily *β*,*δ*-selectivity in the cleavage of heme (Wang, J., Evans, J. P., Ogura, H., La Mar, G. N., and Ortiz de Montellano, P. R. (2006) *Biochemistry 45*, 61−73). The ^{1}H NMR hyperfine shift pattern for the substrate and axial His C_βH's and the substrate−protein contacts of the cyanide-inhibited protohemin and 2,4-dimethyldeuterohemin complexes of the triple mutant have been analyzed in detail and compared to data for the WT complex. It is shown that protein contacts for the major solution isomers for both substrates in the mutant dictate ∼90° in-plane clockwise rotation relative to that in the WT. The conventional interpretation of the pattern of substrate methyl hyperfine shifts, however, indicates substrate rotations of only ∼50°. This paradox is resolved by demonstrating that the axial His25 imidazole ring also rotates counterclockwise with respect to the protein matrix in the mutant relative to that in the WT. The axial His25 C_βH hyperfine shifts are shown to serve as independent probes of the imidazole plane orientation relative to the protein matrix. The analysis indicates that the pattern of heme methyl hyperfine shifts cannot be used alone to determine the in-plane orientation of the substrate as it relates to the stereospecificity of heme cleavage, without explicit consideration of the orientation of the axial His imidazole plane relative to the protein matrix.

Heme oxygenase, HO,[1] is a nonmetal enzyme that uses protohemin, PH, as both a cofactor and a substrate to produce biliverdin, iron, and CO (*1*, *2*), as illustrated in Figure 1. In mammals, all three products of the ∼300-residue, membrane-bound enzyme have key roles, biliverdin as the precursor to the powerful antioxidant bilirubin (*3*), CO as a gaseous neural messenger (*4*), and the iron in iron homeostasis (*5*). In plants and cyanobacteria, the soluble HO-cleaved tetrapyrrole serves as a precursor to light-harvesting pigments (*6*), while in some pathogenic bacteria soluble HOs appear to act primarily to "mine" iron from host hemoglobin (*7*, *8*). While sequence homology is limited, all HOs appear to act via the pathway depicted in Figure 1, except that the cleavage does not always occur at the α-*meso* position (*2*, *7*, *9*, *10*). Exclusive α-*meso* stereoselectivity is observed (*2*) for mammalian, cyanobacterial, and pathogenic bacterial HOs from *Neisseria meningitidis* (*11*) and *Corynebacterium diphtheriae* (*12*). A prominent exception is the HO from the opportunistic pathogen *Pseudomonas aeruginosa*, *Pa*HO, which uniquely exhibits mixed *β*,*δ*-stereoselectivity (*13*). Crystal structures of a variety of HOs have revealed (*14*−*20*) a common HO fold in spite of significant sequence variations. The stereoselectivity of the reaction can be accounted for by two distinct contributions, the proximity of the distal helix backbone to the heme that blocks three of the four *meso* positions to attack by Fe^{3+}OOH and a distal helix backbone interaction with exogenous iron ligands that tilts/bends/orients this ligand strongly toward the fourth, unblocked *meso* position (*14*−*20*). The variable stereoselectivity among HOs is accounted for by the manner in which heme is "seated" in this conserved active site (*13*−*20*).

Protohemin, PH, seating in HO is controlled by the interaction of the propionate side chains with cationic residue side chains and/or H-bond donors from the protein matrix (*14*−*22*). A schematic depiction of the active site of hHO is given in Figure 2; ring cleavage occurs at the *meso* position between M_b and M_c as marked with an asterisk. The individual heme substituents are not shown, but are identified as a → h that correspond to the positions 1 → 8 for the major isomer in hHO−PH−CN in solution (*23*, *24*) and to positions 4 → 1 and 8 → 5 for the hHO−PH crystal structures (*14*, *15*). In either case, WT-hHO places propionates at positions

† This research was supported by grants from the National Institutes of Health, GM62830 (G.N.L.M.) and DK30297 (P.R.O.d.M.).

* To whom correspondence should be addressed. Fax: (530) 752-8995. E-mail: lamar@chem.ucdavis.edu. Phone: (530) 752-0958.

‡ University of California, Davis.

§ University of California, San Francisco.

[1] Abbreviations: HO, heme oxygenase; hHO, soluble 265-residue construct of human heme oxygenase-1; TM-hHO, hHO triple mutant K18E/E29K/R183E-hHO; *Pa*HO, heme oxygenase from *Pseudomonas aeruginosa*; NOE, nuclear Overhauser effect; NOESY, two-dimensional nuclear Overhauser spectroscopy; TOCSY, two-dimensional total correlation spectroscopy; DSS, 2,2-dimethyl-2-silapentane-5-sulfonate; PH, protohemin; DMDH, 2,4-dimethyldeuterohemin; δ_{con}, contact shift; δ_{hf}, hyperfine shift.

10.1021/bi7017333 CCC: $40.75
Published on Web 12/14/2007

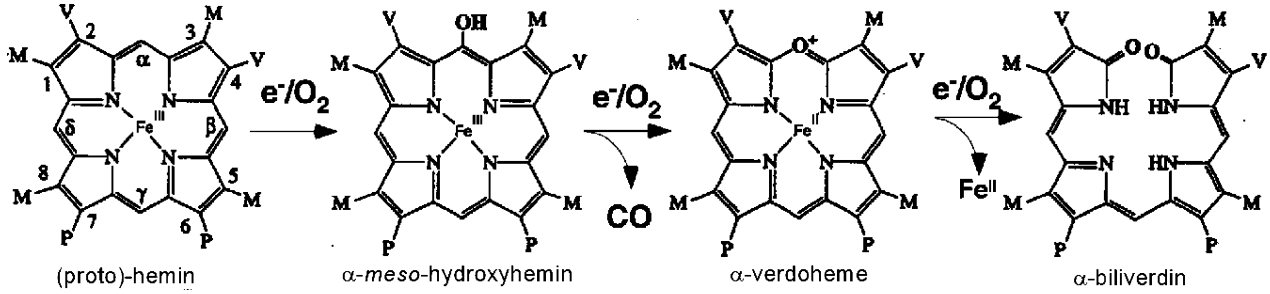

FIGURE 1: The oxidation of protohemin by heme oxygenase is shown for the α-stereoselective mammalian enzyme.

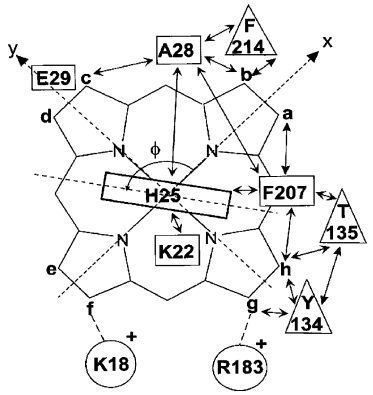

FIGURE 2: Schematic depiction of the active site of an hHO−substrate complex. The substrate substituents are not displayed; instead their positions are labeled a → h, corresponding to the PH positions 1 → 8 for the major isomer of hHO−PH−CN in solution, or 4 → 1 and 8 → 5 for hHO−PH in crystals (*14*, *15*). In either case, positions f and g are occupied by propionates in WT-hHO complexes, and these propionates make salt bridges to Lys18 and Arg183 (shown by dashed lines). Glu29, which must be mutated (*27*) to allow 90° in-plane rotation of the substrate, is also shown. The positions of key residues in contact with the substrate and the axial His25 are shown as rectangles (proximal side) or triangles (equatorial to the heme), and the double-sided arrows reflect the expected (*14*, *15*) and observed (*23*, *24*, *34*) NOESY contacts between individual substrate positions and these residues, as well as among these residues. The orientation of the axial His25 imidazole plane relative to the substrate *x*-axis that passes between positions a and b is indicated by the angle ϕ (∼125° in crystals). It is important to note that the *reference coordinate system is tied to the porphyrin, and not to the protein matrix.*

f and g, whose carboxylates participate in salt bridges (represented by dashed lines in Figure 2) to the key cationic termini of Lys18 and Arg183, respectively. Thus, β-versus α-stereoselectivity results (*13*, *20*) from an in-plane, ∼90° clockwise rotation of PH (as shown in Figure 3B) in *Pa*HO relative to that in the more common α-selective HOs (as shown in Figure 3A; methyl = M, vinyl = V, and propionate = P). The factors that determine the precise orientation of the substrate in HOs, and hence the cleavage stereoselectivity, are of significant current interest (*13*, *20*, *25*−*27*).

While only a single heme orientation is detected in crystal structures (*14*−*20*), NMR studies revealed that PH, in general, occupies two orientations (*13*, *23*, *28*, *29*) differing by a 180° rotation about the α,γ-*meso* axis, as depicted in Figure 3A,D for hHO, which are comparably populated upon the initial binding of substrate (*23*, *29*). This natural α,γ-*meso* orientational isomerism completely conserves α-stereoselectivity in mammalian and bacterial α-selective HOs, but results in mixed β,δ-stereoselectivity (*13*, *20*) in *Pa*HO due to hemin rotated in-plane by 90° relative to that in α-stereoselective HOs. This α,γ-*meso* orientational isomerism of PH in HO is not detected in crystals (*14*−*20*), but it is readily detected in NMR spectra (*13*, *23*−*32*). The orientation of PH relative to the protein matrix in WT-hHO, as represented by the position of Ala28 and Phe207 in the crystal (*14*, *15*) and the major isomer in solution (*23*), is depicted in parts A and D, respectively, of Figure 3.

For proper characterization of HOs with mixed and/or altered stereospecificity, it is necessary to critically assess and improve the physical methods which will clearly resolve the molecular heterogeneity that is the basis for the mixed stereoselectivity, as well as provide detailed information on substrate seating within each isomer. The elucidation of heme seating in solution of the cyanide-inhibited substrate−HO complexes has been pursued by two distinct approaches. The natural paramagnetism of these complexes leads (*33*) to large hyperfine shifts, δ_{hf}, but only minor enhanced relaxation, that allow ready assignment of both substrate and active site proton signals by conventional ^{1}H 2D NMR (*33*). On one hand, upon separate assignment of the substrate and multiple key active site residue signals, the substrate orientation relative to the protein matrix is established by the detailed pattern of residue−substrate NOESY cross-peaks (*23*, *27*, *31*, *34*). The hyperfine shifts simply provide improved resolution for the target signals.

The alternate approach rests on the distinctive pattern of substrate methyl hyperfine shifts that, in a low-spin ferric cyanide/His hemoprotein with the $(d_{xy})^2(d_{xz},d_{yz})^3$ orbital ground state, directly reflects (*13*, *26*, *32*, *33*, *35*) the orientation of the axial His imidazole plane, relative to the hemin N−Fe−N vector defined by the angle ϕ, as shown in Figure 2. The pattern of methyl shifts has been semiquantitatively related[3] (*35*, *36*) to ϕ, and for the alternate orientations of PH about its α,γ-*meso* axis (where the rhombic effects of vinyl groups must also be considered) and for the synthetic pseudocentrosymmetric substrate 2,4-dimethyldeuterohemin (DMDH), the patterns are illustrated[2,3] in parts A, B, and C, respectively, of Figure 4. These empirical curves in Figure 4 account reasonably well for the

[2] It is important to emphasize that the relations depicted in Figure 4 require that the axis to which the angle ϕ is tied is not the stationary protein matrix, but must be rotated with the substrate, as shown in the series parts A, B, and C of Figure 3.

[3] The graphs for predicted hyperfine shifts, δ_{hf}, versus the angle between the axial His imidazole plane and the N_A−Fe−N_C vector, ϕ, were generated using the program Shift Patterns v.2, written by Shokhirev and Walker (*35*) (available from http://shokhirev.com/nikolai/programs/prgsciedu.html, accessed Oct 16, 2006) for the essentially centrosymmetric DMDH (Figure 4C) and adapted to the crystallographic PH orientation (*14*) (Figure 4A) and dominant solution PH orientation (*23*) (Figure 4B) by adding upfield bias for the methyls adjacent to 2- and 4-vinyl groups relative to that in DMDH, as discussed by Shokhirev and Walker (*35*).

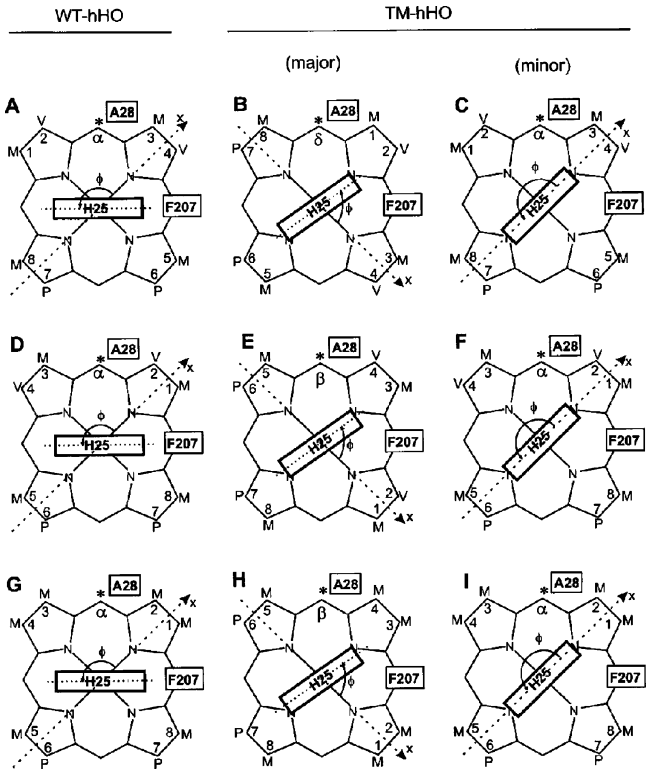

FIGURE 3: Schematic depiction of the orientations, relative to the protein matrix, of the substrate and axial His imidazole plane in the WT- and TM−hHO complexes. The substrate methyl, vinyl, and propionate substituents are shown as M, V, and P, respectively. Shown are the conserved positions of Ala28 and Phe207, the two key residues that define the substrate orientation relative to the protein matrix, and the angle ϕ between the axial His25 imidazole plane and the substrate N−Fe−N vector (*x*-axis, tied to the substrate) that defines the His plane orientation relative to the substrate. The two substrates of interest are PH (2V, 4V) and DMDH (2M, 4M). The *meso* position that is cleaved in each case on the basis of the seating in the protein matrix is labeled with an asterisk. (A), (D), and (G) show the substrate orientation in WT-hHO for (A) PH oriented about the α,*γ-meso* axis as in the crystal (*14*) (and in the major isomer of TM−hHO), (D) PH rotated by 180° about the α,*γ-meso* axis relative to those in (A), as in the major solution isomer of hHO−PH−CN (*23*), and (G) DMDH in its unique orientation in hHO−DMDH−CN (*39*). The axial His25 imidazole orientation in each case is that observed in the crystal (*14*). (B), (E), and (H) display the substrate rotated clockwise ∼90° in-plane and the axial His imidazole plane rotated ∼40° counterclockwise relative to those in the WT (A, D, and G, respectively) as the candidates for the major solution isomer in TM−hHO complexes. (C), (F), and (I) show the substrates with conserved orientation but with the axial His25 imidazole plane rotated ∼40° counterclockwise relative to that of the WT (A, D, and G, respectively) as candidates for the minor solution isomers of TM−hHO. The orientation of the substrate relative to the protein matrix is determined by either crystallography or solution substrate-to-protein NOEs; the orientation of the axial histidine relative to the substrate (ϕ) was determined by the empirical methyl and His25 $C_\beta H$ δ_{hf} patterns.

observed heme methyl shifts in characterized ferrihemoproteins (*33*, *35*, *37*, *38*). Hence, the relations in Figure 4 have been gainfully utilized to determine the in-plane heme seating deduced in WT-*Pa*HO (*13*) and in a variety of mutants (*26*, *32*) with perturbed protein contacts to the heme propionates. In general, a good correlation between deduced PH orientation and biliverdin isomer production is observed. An implicit assumption in interpreting the substrate methyl ^1H or ^{13}C hyperfine shifts in terms of hemin seating in the active site

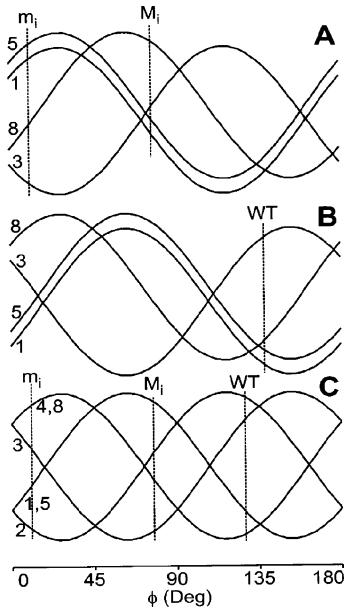

FIGURE 4: δ_{DSS}(calcd) for (A) PH oriented about the α,*γ-meso* axis as in Figure 3A−C (as in the crystal (*14*)), (B) for PH oriented about the α,*γ-meso* axis as in Figure 3D−F (as in the major isomer in solution (*23*)), and (C) for DMDH, labeled as in Figure 3G−I, as a function of the angle ϕ between the axial His25 imidazole plane and the *x*′-axis that lies along the N_A-Fe-N_C vector in the crystallographic orientation of PH (Figure 3A) and along the N_B-Fe-N_D vector in the solution orientation of PH (Figure 3B) and DMDH (Figure 3G), as described[3] by Shokhirev et al. (*35*). The vertical dashed lines headed by WT, M_i, and m_i, correspond to the ϕ values that are consistent with the methyl δ_{hf} pattern in the WT, mutant major isomers, and mutant minor isomers, respectively.

via the angle ϕ is that the orientation of the axial His imidazole plane relative to the protein matrix is completely conserved. It is the orientation of the hemin relative to the protein matrix, and not relative to the axial His imidazole plane, that is the determinant of the stereoselectivity of the HO reaction.

We have shown recently (*27*) that replacing the native, cationic Lys18 and Arg183 that interact with the propionates with anionic side chains (Glu) leads to ∼50% α- and ∼50% mixed β,δ-stereoselectiveity, indicating ∼50% ∼90° in-plane reorientation of PH in the pocket. To induce dominant β,δ-stereoselectivity (>90%), it was necessary (*27*) to additionally replace the native anionic Glu29, which serves as an acceptor to the axial His ring $N_\delta H$, with Lys (to generate the triple mutant K18E/E29K/R183E-hHO ≡ TM-hHO) to stabilize propionate interactions in a ∼90° in-plane rotated PH. Solution ^1H NMR spectra of TM-hHO−PH−CN revealed (*27*) four equilibrium isomeric forms in the ratio 50:5:25:20, with rapid interconversion within the first and last pairs. The orientation of PH in the major isomer was established (*27*) on the basis of NOEs between PH and characteristically (*23*, *24*, *39*) hyperfine shifted active site residues, shown schematically in Figure 2. The NMR data revealed that the major isomer (∼50%) orients PH about the α,*γ-meso* axis as found in the crystal (*14*, *15*), but exhibits a ∼90° clockwise, *in-plane* rotation (*27*) (viewed from the proximal side) relative to that in WT-hHO−PH−CN (Figure 3A), as shown in Figure 3B, while the PH orientation for the minor equilibrium isomer (∼5%) was suggested to be that in the hHO−PH−H_2O crystal (Figure 3C). The other two isomers interconverted too rapidly to be assigned but

were proposed (*27*) to arise from the alternate orientation of PH about the α,γ-*meso* axis (Figure 3E,F). Hence, it was not possible to directly monitor the relative thermodynamic stabilities (populations) of the "native" and ~90° in-plane rotated PH. Last, we noted that the pattern of methyl hyperfine shifts for the major isomer of TM-hHO−PH−CN was inconsistent with the deduced 90° in-plane rotation of PH.

This latter observation (*27*) demands a re-examination of the relationships among changes in the substrate hyperfine shift pattern, in-plane seating of substrates in HO complexes, and the orientation of the axial His imidazole plane in TM-hHO. We present here a detailed analysis of the substrate and axial His hyperfine shifts of TM-hHO−PH−CN for the two interconverting isomers whose resonances were assigned (*27*) and expand our studies to the cyanide complex of the DMDH (*39*) (Figure 3G−I) whose 2-fold symmetry about the α,γ-*meso* axis obviates the usual α,γ-*meso* orientational isomerism in TM-hHO−PH−CN and hence allows direct determination of the relative thermodynamic stabilities of propionate−protein interactions in the native and ~90° in-plane rotated substrate. The disparity between the in-plane PH orientation deduced from the alternate NMR approaches is shown to be consistent with a rotation of the axial His imidazole plane that is conveniently monitored by the His $C_\beta H$ δ_{hf} pattern.

EXPERIMENTAL PROCEDURES

TM-hHO. The triple mutant K18E/E29K/R183E-hHO (=TM-hHO) is the same as that reported previously (*27*). The complex of DMDH (Figure 3G−I) was prepared by addition to the apoprotein of a stoichiometric amount of DMDH (*39*), followed by chromatography on Sephadex G25. A 10-fold molar excess of KCN was added to yield a ~1 mM TM-hHO−DMDH−CN solution in ^2H_2O, 50 mM phosphate; the pH in ^2H_2O is uncorrected and is presented as p^{2}H (~7.1).

NMR Spectroscopy. ^{1}H NMR data were recorded on a Bruker AVANCE 600 spectrometer operating at 600.16 MHz. Reference spectra were collected over the temperature range 3−25 °C at a repetition rate of 1 s^{-1} over a sweep width of 70 ppm. NOESY spectra (*40*, *41*) were recorded at 3 and 5 °C over a sweep width of 64−70 ppm, at a repetition rate of 2 s^{-1} and a mixing time of 40 ms, and at 20 °C over a sweep width of 22 ppm, at a repetition rate of 1 s^{-1} and a mixing time of 40 ms, using 512 blocks of 1024 data points. 2D data sets were processed with 45−60°-sine-squared-bell apodization in both dimensions and zero field to 2048 × 2048 data points prior to Fourier transformation.

HPLC Analysis of Biliverdin Isomers. The regiospecificities of the reactions by hHO−DMDH and TM-hHO−DMDH were determined in the presence of catalase and superoxide dismutase according to published methods (*27*). An authentic DMDH−biliverdin dimethyl ester mixture was prepared directly from DMDH by coupled oxidation followed by hydrolysis as described by Bonnett et al. (*42*).

RESULTS

Molecular Heterogeneity of TM-hHO Complexes of PH and DMDH. The resonances from TM-hHO−PH at 20 °C in Figure 5A have been shown to arise from four isomers in an approximate ratio of 50:5:25:20, with assignments reported only for the first of the two interconverting pairs (*27*). The methyl peaks are labeled M_i and m_i for methyls (at position *i* in the substrate skeleton in Figure 3A) for the interconverting ~50% and ~5% isomers, respectively, as reported previously (*27*) on the basis of spatial contacts between PH and the assigned protein matrix for the major isomer. The methyl peaks for the remaining two interconverting isomers (25%, 20%) of TM-hHO−PH−CN were not assigned and are simply labeled m. The 20 °C ^{1}H NMR spectrum of TM-hHO−DMDH−CN in Figure 5B exhibits only very broad heme methyl lines, which become progressively sharper as the temperature is lowered (part C → part E of Figure 5), resolving two sets of interconverting resonances, labeled M_i and m_i for major and minor isomers, respectively, with the position assignment *i* as determined below. The relative populations of the two isomers gauged from the M_i:m_i intensity ratio at 10 °C is ~3.

Substrate Seating in the Major Isomer of TM-hHO−PH−CN. We had shown (*27*) qualitatively that the NOEs experienced by M_3 and M_1 in TM-hHO−PH−CN were very similar to those previously reported for M_5 and M_3, respectively, in WT-hHO−PH−CN, indicating an approximately 90° clockwise, in-plane PH orientation in the mutant (Figure 3B) relative to the WT (Figure 3A). A more quantitative analysis of the predicted and observed NOESY intensity ratios between Ala28 $C_\beta H_3$ and substrate methyls M_b and M_c (not shown; see the Supporting Information) confirms a 90° rotation (within ±5°), i.e., $\Delta\phi = \phi_{WT} - \phi_{TM} \approx 90°$.

The predicted[2,3] (*35*) patterns of methyl δ_{hf} for PH as a function of the angle, ϕ, between the N−Fe−N vector and the plane of the His25 imidazole are shown in parts A and B of Figure 4 for the alternate PH orientations about the α,γ-*meso* axis, as found in the hHO−PH−NO crystal structure (*14*), and for the dominant isomer in solution of WT-hHO−PH−CN (*23*), respectively. The WT-hHO−PH−CN substrate methyl chemical shifts are reproduced (*23*) in Table 1 and exhibit the pattern $M_3 > M_8 > M_5 > M_1$, which indicates $\phi \approx 135°$ (vertical dotted line under "WT" in Figure 4B), which is in reasonable accord (130 ± 5°) with the value $\phi \approx 125°$ observed in crystal structures (*14*, *15*).

The methyl chemical shifts for the two assigned isomers of TM-hHO−PH−CN are provided (*27*) in Table 1. The major isomer exhibited the pattern $M_8 > M_5 > M_3 > M_1$, which indicates $\phi \approx 80°$ (vertical dotted line under "M_i" in Figure 4A). The methyl hyperfine shift patterns predict *differences* in ϕ, $\Delta\phi$, between the WT-hHO and the TM-hHO major isomer, $\Delta\phi \approx 130° - 80° \approx 50°$ for PH. Thus, the methyl hyperfine shift pattern alone predicts only a ~50° difference in the in-plane rotational seatings of the PH for the major isomers of TM-hHO and WT-hHO, in contrast to the 90° difference determined by NOESY contacts to the protein matrix.

Substrate Seating in the Major Isomer of TM-hHO−DMDH−CN. DMDH does not possess a unique numbering in the Fischer notation. However, we will assign the numbering as shown in Figure 3G−I, which is the same as that used to establish the assignments in the WT-hHO−DMDH−CN complex (*39*). The structure of the substrate requires the inter-methyl NOESY cross-peaks around the substrate periphery as M_8−M_1 (weak, w), M_1−M_2 (moderate, m), M_2−M_3 (w), M_3−M_4 (m), and M_4−M_5 (w). The NOESY

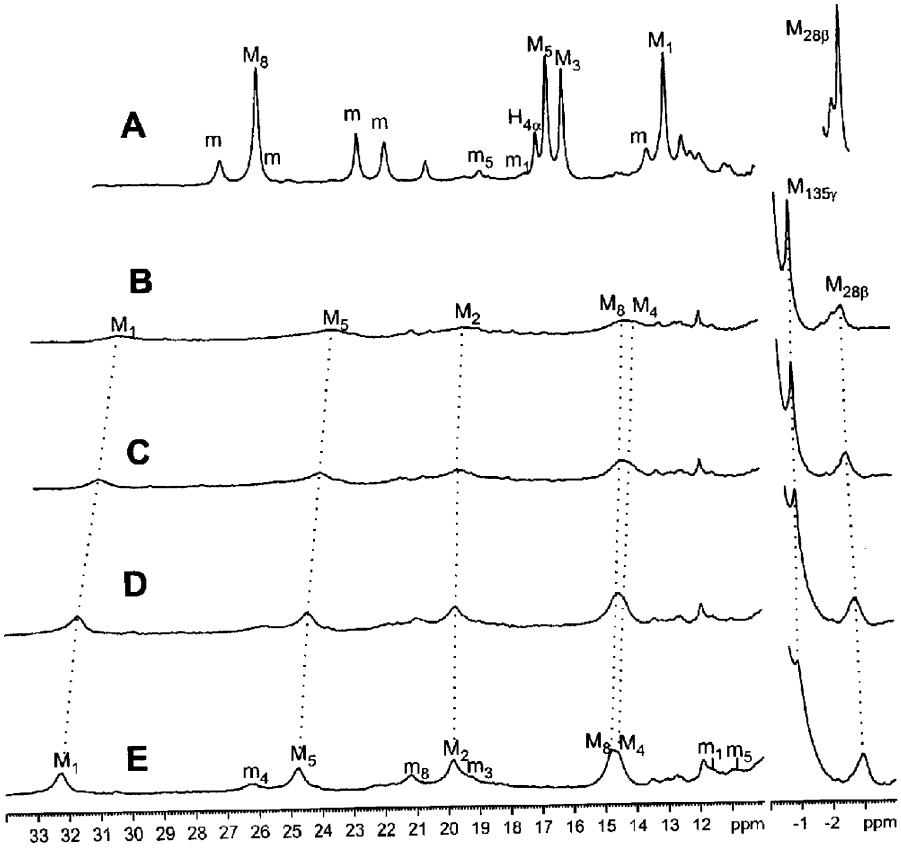

FIGURE 5: Resolved portions of the 600 ^{1}H NMR reference spectra in ^2H_2O, 50 mM phosphate, p^{2}H 7.1, of (A) TM-hHO−PH−CN, at 20 °C, with four isomers present with methyl (single proton) peaks M_i (H_i) and m_i, where *i* represents the methyl (single proton) assignment for the interconverting major (50%) and minor (5%) isomers (*27*) (peaks for the other two isomers are labeled simply m), and (B−E) TM-hHO−DMDH−CN at (B) 20 °C, (C) 15 °C, (D) 10 °C, and (E) 5 °C. Methyl peaks are labeled by M_i and m_i (and single protons H_i and h_i) for the major and minor isomers, respectively, where *i* represents the position in DMDH as defined in Figure 3G−I or the residue number.

spectrum at 10 °C revealed the expected five dipolar connectivities between pairs of the six methyls of the major isomer (not shown; see the Supporting Information) and exchange cross-peaks (*43*) to each of the minor isomer methyl peaks; the methyl chemical shifts of the two isomers are included in Table 1. Line broadening interfered with TOCSY spectra but conserved intra- and interresidue NOESY contacts among residues with conserved δ_{hf} in the major isomer locate the signals for all key residues (not shown; see the Supporting Information) assigned in TM-hHO−DMDH−CN (*27*) except the axial His25. Chemical shifts are listed in Table 1. The pattern of residue−DMDH NOESY cross-peaks (not shown; see the Supporting Information) are consistent with an in-plane, ~90° rotated DMDH relative to the WT, which is confirmed by the ratio of Ala28 $C_\beta H_3$ to M_1 and M_8 NOESY cross-peaks (not shown; see the Supporting Information).

The predicted (*35*) methyl chemical shift versus ϕ for DMDH as the substrate is illustrated in Figure 4C. For the WT complex, the DMDH methyl shift pattern (Table 1) (*39*) is $M_2 > M_3 > M_5 \approx M_8 > M_1 > M_4$, which predicts $\phi \approx 130°$ (vertical dotted line under "WT" in Figure 4C), which is very similar to the 125° observed in the crystal (*14*). For the major isomer of TM-hHO−DMDH, the observed (Table 1) shift pattern, $M_1 > M_5 > M_2 > M_4 \geq M_8 > M_3$, predicts[2,3] $\phi \approx 80°$ (vertical dotted line under "M_i" in Figure 4C). The methyl hyperfine shift patterns predict differences in ϕ, $\Delta\phi$, between the WT-hHO and TM-hHO major isomer, $\Delta\phi \approx$

Table 1: Chemical Shifts for Active Site Residues for TM- and WT-hHO−Substrate Complexes[a]

	PH[b]			DMDH[c]		
	WT-hHO[d]	TM-hHO[e]		WT-hHO[f]	TM-hHO[g]	
residue	M_i	M_i	m_i	M_i	M_i	m_i
heme M_1	4.43	12.69	17.00	8.86	32.22	11.78
heme M_2				22.61	19.83	8.12
heme M_3	19.63	15.95	10.89	19.13	4.65	19.32
heme M_4				8.12	15.54	26.16
heme M_5	9.04	16.37	18.33	7.93	24.74	20.88
heme M_8	10.48	25.21	12.69	9.74	14.81	21.20
His25 $C_{\beta 1}H$	9.99	9.07		10.62		
His25 $C_{\beta 2}H$	9.24	12.04		8.88		
Ala28 $C_\beta H_3(M_{28\beta})$	−2.25	−2.15		−2.67	−2.97	
Ala28 $C_\alpha H$	2.25	2.45		2.13	2.15	
Tyr134 $C_\delta H$	6.71	6.77		6.64	6.64	
Tyr134 $C_\epsilon Hs$	6.45	6.60		6.14		
Thr135 $C_\gamma H_3$	0.01	−0.51		−0.32	−0.98	
Phe207 $C_\delta H$	6.50	5.27		5.79	4.80	
Phe207 $C_\epsilon H$	5.85	6.13		6.31	5.84	
Phe214 $C_\delta Hs$	6.62	6.41		6.12	6.42	
Phe214 $C_\epsilon H$	6.95	6.54		6.23	6.63	
Phe214 $C_\xi H$	7.78	7.06		6.85	7.24	

[a] In parts per million, referenced to the peak for DSS, in ^2H_2O, 50 mM phosphate at p^{2}H 7.0. [b] Protohemin. [c] 2,4-Dimethyldeuterohemin. [d] At 30 °C for PH oriented as in Figure 3D (*23*, *24*). [e] At 25 °C for PH with M_i and m_i oriented as in parts B and C, respectively, of Figure 3 (*27*). [f] At 10 °C for DMDH oriented as in Figure 3G (*39*). [g] At 10 °C M_i and m_i for DMDH oriented as in parts B and C, respectively, of Figure 3 as determined herein.

130° − 80° ≈ 50° for DMDH. Hence, for both PH and DMDH complexes of TM-hHO, the orientation of the substrate deduced from NOESY contacts to the assigned protein matrix indicates the substrate is in-plane rotated ~90° clockwise in TM-hHO relative to the WT-hHO complex. In contrast, the orientations of either PH or DMDH deduced from the patterns of the substrate methyl hyperfine shifts indicate only a ~50° in-plane rotation of the substrate in the mutant relative to WT-hHO. It is unlikely that the discrepancy between the substrate in-plane orientation deduced from spatial contacts (NOESY connections to the protein matrix) and the empirical correlation between the methyl hyperfine shift pattern and ϕ (Figure 4) reflects a serious shortcoming in either procedure. Rather, it suggests that yet another variable, the orientation of the His25 imidazole plane, differentiates the WT- and TM-hHO complexes.

Stereospecific Assignment of the Axial His25 C_βH's in TM-hHO−PH−CN. The orientation of the axial His relative to the protein matrix is suitably probed by the uniquely assigned[4] His25 C_βH signals, which must be stereospecifically assigned. Such assignment of the His25 C_βH's in TM-hHO−PH−CN rests on the predicted much closer proximity of $C_{\beta1}$H than $C_{\beta2}$H to the Lys22 backbone C_αH (the α_i−β_{i+3} helical connection (*14*, *39*, *44*). The relative His25 C_βH to Lys22 C_αH distances cannot be significantly altered for any His25 ring orientation that maintains an iron His25 bond on an intact proximal helix. For WT-hHO−PH−CN the two His25 C_βH's have been shown (*24*) to exhibit similar shifts, with $C_{\beta1}$H at lower field (by ~0.7 ppm, not shown; see the Supporting Information) and exhibiting the expected strong NOEs to Lys22 C_αH. Portions of the NOESY spectrum of TM-hHO−PH−CN displaying the key His25/Lys22 contacts, depicted in Figure 6, reveal His25 C_βH's with much larger shift differences (~3 ppm) and with the $C_{\beta1}$H signal, with the stronger contact to Lys22 C_αH, resonating at higher field. Thus, the two His25 C_βH's interchange the relative magnitudes of the low-field bias and are more strongly differentiated in the mutant than the WT complex. The chemical shifts for His25 are listed in Table 1.

DMDH Cleavage Stereospecificity. The P450 reductase-catalyzed reaction of hHO−PH typically produces exclusively α-biliverdin (*2*). Coupled oxidation of DMDH leads to all four biliverdin isomers, for which the 2-fold symmetry of DMDH leads to identical isomers upon cleavage of either the β- or δ-position (Figure 7A); we describe the three possible isomers as α-, $\beta(\delta)$-, and γ-biliverdin. The WT-hHO complex of DMDH maintains α-selectivity (>99%) (Figure 7B). Superoxide dismutase and catalase were included in all of the assays to ensure that no hydrogen peroxide was involved in the alteration of regiospecificity. The TM-hHO−DMDH complex, with an observed ratio of 11% α- and 89% $\beta(\delta)$-biliverdin (Figure 7C) favored greater in-plane rotation than the TM-hHO−PH complex with 16% α- and a combined 84% β- and δ-isomers (*27*). In the coupled oxidation there was an effect on the regiospecificity of the reaction similar to that observed in the P450 reductase catalyzed reaction, except to a greater degree. The WT-hHO−DMDH maintains α-selectivity (Figure 7D) while TM-hHO−DMDH produces as much as 96% β-isomer (Figure 7C), compared to a combined 90% β- and δ-isomers for the TM-hHO−PH complex.

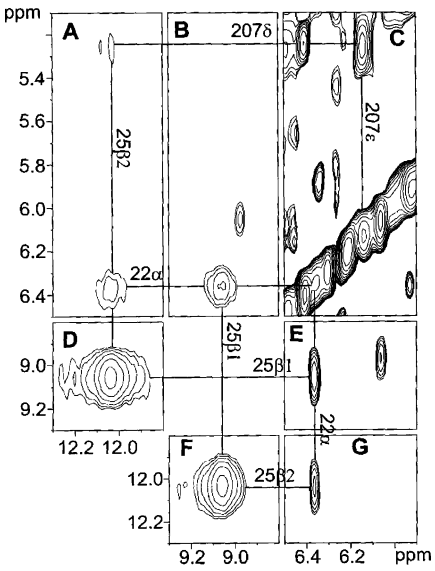

FIGURE 6: Portion of the 600 MHz ^{1}H NMR NOESY spectrum of TM-hHO−PH−CN in ^2H_2O, 50 mM phosphate, p^{2}H 7.1, at 5 °C depicting the His25 C_βH contacts (A) to Phe207, (A, B, E, G) to Lys22 C_αH, and (D, F) between the two His25 C_βH's. The stronger contact with Phe207 C_δH and weaker contact to Lys22 C_αH identify the lower field His C_βH as $C_{\beta2}$H in the crystal (*14*, *15*).

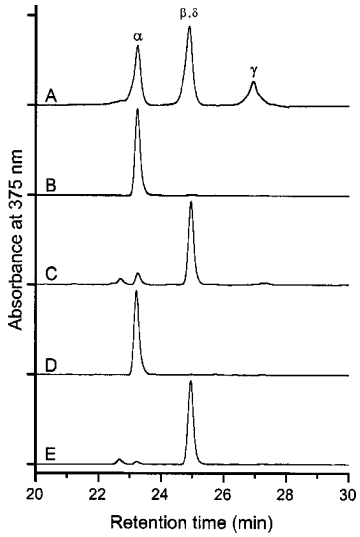

FIGURE 7: Regiospecificity of hHO−DMDH and TM-hHO−DMDH as determined by HPLC analysis of biliverdin dimethyl esters. (A) Three isomers obtained in the coupled oxidation of DMDH. The P450 reductase supported reaction of hHO−DMDH produces >99% α-isomer (B), while TM-hHO−DMDH produces 11% α- and 89% β-isomers (C). The sodium ascorbate supported oxidation of hHO−DMDH produces >99% α-isomer (D), while TM-hHO−DMDH produces 4% α- and 96% β-isomers (E).

DISCUSSION

Heme In-Plane Rotational Preference. The relative intensities of the M_i:m_i peaks, ~3:1 in TM-hHO−DMDH−CN,

[4] The axial His C_βH's in a large variety of His/CN$^-$-ligated ferrihemoproteins (*33*) and the heme propionate C_αH's are the only strongly coupled and relaxed protons that give rise to signals to the low field of ~9 ppm. The absence of NOESY cross-peaks of such a geminal pair of protons to either the 5- or 8-methyl peak eliminates the propionates and uniquely identifies the axial His C_βH's (*33*). The most intense NOESY cross-peak to the His C_βH's in HOs is from the C_αH of the residue three residues closer to the N-terminus (*39*).

indicate that, for the cyanide-inhibited complex, the ~90° in-plane rotated (Figure 3H) substrate is 0.7 kcal more stable than that with the propionate in the more "native" orientation (Figure 3G,I). For PH, only two isomers have been characterized, those comprising ~50% and 5%, with orientations as in parts B and C, respectively, of Figure 3. The two remaining, comparably populated (25%, 20%), interconverting isomers can be assumed to represent the isomers depicted in Figure 3E,F. Thus, we can conclude that ~70%/75% of PH in TM-hHO−PH−CN is in-plane rotated ~90° from that found for the WT in either solution (Figure 3D) or the crystal (Figure 3A) (the two differing only in a 180° rotation about the α,γ-*meso* axis) and ~30%/25% of PH exists with the propionates oriented similarly to those in the WT (Figure 3C,F, differing only in 180° rotation about the α,γ-*meso* axis). Thus, the preference between the native propionate positions and those with the substrate rotated clockwise by ~90° is similar for DMDH and PH.

Axial His25 Imidazole Ring Rotation Relative to the Protein Matrix. $\Delta\phi \approx 90°$ for the substrate relative to the protein matrix and a $\Delta\phi \approx 50°$ orientation of the substrate relative to the His25 ring plane in the major isomers of TM-hHO complexes, when compared to WT-hHO complexes, dictate that the His25 ring must have rotated counterclockwise in TM-hHO (Figure 3B,H) relative to WT-hHO complexes (Figure 3A,G). To establish such a His ring rotation, an independent probe of the orientation of the axial His ring relative to the protein matrix is needed. The contact shift contribution, δ_{con}, to δ_{hf} of $C_\beta H$'s for a ligated His exhibits the characteristic angular dependence on Ψ of methylene protons attached to any π-spin-containing aromatic ring given by (*33*, *45*)

$$\delta^i_{con} \propto (C + D\cos^2\Psi_i) \qquad (1)$$

where Ψ is the dihedral angle between the $C_\pi-C_\beta-H$ plane and the normal to the imidazole plane through C_π and *C* and *D* are constraints with $D > C$. The expected positive π spin density (*33*, *45*) at the imidazole C_γ will result in low-field $C_\beta H$ δ_{con}. The view along the $C_\gamma-C_\beta$ vector of the His25 ring that allows visualization of the $C_\gamma-C_\beta-H$ angles and their changes upon rotating the ring is depicted in Figure 8. In the WT-hHO crystal structure (*14*, *15*), the two His25 $C_\beta H$'s have $\Psi_1(C_{\beta1}H) \approx 55°$ and $\Psi_2(C_{\beta1}H) \approx 65°$ (Figure 8A) for which eq 1 predicts a slightly larger low-field δ_{con} for $C_{\beta1}H$ than $C_{\beta2}H$. The dipolar shift, δ_{dip}, calculated on the basis of published (*39*, *46*) magnetic axes reveals comparable low-field δ_{dip} for the two $C_\beta H$'s. The slightly stronger low-field bias, and hence slightly larger δ_{con}, for $C_{\beta1}H$ than $C_{\beta2}H$ in the WT complex is consistent with the crystal structure. It is noted that, in TM-hHO−PH−CN, the pattern of the His25 $C_\beta H$ δ_{hf} (Figure 6, Table 1) differs dramatically from that of WT-hHO−PH−CN (*33*) (Table 1; see the Supporting Information). δ_{hf} is significantly larger for $C_{\beta2}H$ and significantly smaller for $C_{\beta1}H$ in the TM-hHO−PH−CN complex than in the WT-hHO−PH−CN complex. The decrease in $C_{\beta1}H$ and increase in $C_{\beta2}H$ contact shifts in the TM-hHO−CN complex relative to the WT-hHO−PH−CN complex dictate that Ψ_1 has increased and Ψ_2 has decreased in the mutant relative to the WT complex, as depicted qualitatively in part A → part B of Figure 8.

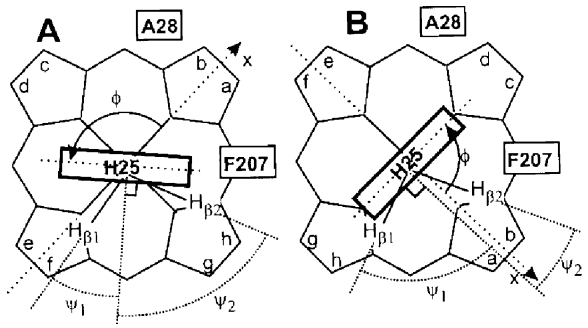

FIGURE 8: Depiction of the influence of rotation of the axial His25 imidazole plane relative to the protein matrix on the dihedral angles Ψ_1 and Ψ_2 between the His25 $C_{\beta1}H$ and $C_{\beta2}H$ relative to the normal of the imidazole plane (dashed line) (A) as found in the crystal structure (*14*, *15*) and conserved in solution (*23*, *24*) with χ_1 slightly smaller than χ_2 and hence a larger low-field contact shift for $C_{\beta1}H$ than $C_{\beta2}H$ as observed (Table 1) and (B) as predicted when the His25 imidazole plane is rotated counterclockwise ~40°, which results in a much smaller χ_2 (and hence larger low-field contact shift) for $C_{\beta2}H$ than $C_{\beta1}H$, as observed (Table 1). The ~40° rotation of the imidazole ring requires a ~5° rotation about the α−β bond to conserve the His−Fe bond, but this α−β bond rotation has only a minor effect on the χ_1 and χ_2 values.

A more quantitative use of the axial His $C_\beta H$ hyperfine shifts in terms of Ψ_1 and Ψ_2 is not possible at this time. It would require both the relative values of *C* and *D* in eq 1, for which only some estimates are available (*33*, *45*), and the magnetic axes of the mutant to quantitate δ_{dip}, for which the needed assignments are compromised by line-broadening and spectral congestion. Nevertheless, the dramatically altered δ_{hf} pattern of His25 $C_\beta H$ in TM-hHO relative to WT-hHO complexes provides clear proof for the counterclockwise rotation of the His25 imidazole plane, as depicted in part A → part B of Figure 8. If we accept that relations between substrate methyl hyperfine shifts in Figure 4 are valid, then the magnitude of the imidazole plane rotation is concluded to be ~40° for each of the complexes of TM-hHO as depicted in Figure 3B,C,E,F,H,I.

It was not possible to detect (*27*) the intraresidue cross-peaks for His25 $C_\beta H$'s in the major isomer TM-hHO−DMDH−CN. However, the much larger exchange contribution to the line width in the DMDH than PH complexes, together with a smaller chemical shift difference between the two isomers for His25 $C_\beta H$'s than substrate methyls, likely places the His25 $C_\beta H$'s in the intermediate chemical exchange limit for the DMDH complex of TM-hHO and renders their signals too broad to detect in the limited accessible temperature range. However, the essentially identical $\phi \approx 80°$, and hence $\Delta\phi \approx 50°$ upon mutation, deduced from the methyl δ_{hf} pattern in both the PH and DMDH complexes of the mutant, argues for very similar axial His ring plane orientations in TM-hHO−PH−CN and TM-hHO−DMDH−CN.

Estimation of the Substrate Orientation in the Minor Isomers of TM-hHO. We note that the strong contribution of exchange to the methyl line width of the minor isomers in equilibrium with the major isomers of TM-hHO for both PH and DMDH precludes a direct determination of the orientation relative to the protein matrix. The patterns of methyl shifts, $M_8 > M_5 > M_3 > M_1$ for PH and $M_4 > M_8 > M_5 > M_3 > M_1 > M_2$ for DMDH, in the minor isomers of TM-hHO yield $\phi \approx 10°$ (or $\phi \approx 190°$, not far from the

180° shown in Figure 3C,I) for both substrates, as illustrated by vertical dotted lines under "m_i" in parts A and C, respectively, of Figure 4. If we assume that the axial His25 imidazole ring is rotated ~40° clockwise in the minor isomers compared to the major isomer of TM-hHO, then the structure would be as illustrated in Figure 3C for the PH and Figure 3I for the DMDH minor isomers. Alternatively, the difference in ϕ between the major and minor isomers in Figure 4 is ~70° for each substrate, which indicates the minor isomers are oriented close (within 20°), but not identical to, that in the WT complexes. In the absence of direct NOESY contacts to the protein matrix or the pattern of the His25 $C_\beta H$ hyperfine shifts, the substrate orientation for the minor isomer cannot be more accurately described at this time. It is risky to place much emphasis on the observation that $\Delta\phi$ determined from the methyl δ_{hf} pattern for the two substrates is ~70° rather than ~90°. The empirical correlations (*35*) in Figure 4, while providing a useful framework for estimating ϕ, are only semiquantitative and based on a model (*35*) that requires retention of inversion symmetry for methyl δ_{hf} in the protein environment for strictly centrosymmetric substrates, which is not observed for a variety of such substrates (*47*−*49*).

The rapid exchange, even at 5 °C, between the two uncharacterized, interconverting isomers in TM-hHO−PH−CN which give rise to methyl peaks labeled "m" in Figure 5A has precluded the assignment of either the PH methyl peaks or their protein matrix contacts. However, it is reasonable to propose their structures as those depicted in Figure 3E,F.

Stereoselectivity of DMDH Cleavage in WT- and TM-hHO. Two observations are notable. One is that, in WT, both DMDH and PH yield exclusively α-biliverdin. This is consistent with the observation that the in-plane orientation of DMDH and PH in the WT-hHO−cyanide complexes could not be differentiated by ^{1}H NMR. The second is that the ratio of isomers for DMDH cleavage, 89% β/δ- and 11% α-biliverdin, is qualitatively, but not quantitatively, consistent with the 70% and 30% populations of the respective DMDH seatings determined by ^{1}H NMR in the cyanide complex. The latter observation reminds one that the stereoselectivity of the substrate cleavage is determined by the isomeric seating preference in the resting state, aquo complex, and that previous ^{1}H NMR studies (*50*) have shown that the relative stabilities of alternate PH seatings about the α,γ-*meso* axis are different in the aquo and cyano complexes of hHO, with the former exhibiting less orientational preference than the latter complex. A similar difference between biliverdin isomer distribution and PH seating preference in the cyano complex has been noted for *Cd*HO mutants (*32*). The very broad resonances of the high-spin aquo complex make characterization of isomer identity and distribution very difficult, particularly for low-concentration isomers. The very rapid ($>10^2$ s^{-1}) interconversion of the alternate in-plane substrate orientation precludes "trapping" the aquo isomer distribution upon forming the cyano complex.

CONCLUSIONS

Several important conclusions are indicated: (1) The pattern of dipolar contacts between substrate methyls and heme pocket residues, rather than the substrate methyl hyperfine shift pattern, is the less unambiguous indicator of the substrate orientation. (2) The pattern of substrate methyl hyperfine shifts in the mutant can be used to compare the in-plane substrate orientation relevant to the stereoselectivity of substrate cleavage only if it is established that the axial imidazole orientation is conserved. The conservation of the axial His orientation need not be assumed, but can be determined from the pattern of axial His $C_\beta H$ δ_{hf}. (3) As noted previously (*13*, *50*), the distribution of in-plane orientational isomers as detected in the ^{1}H NMR spectra of the cyano complexes is qualitatively, but not quantitatively, related to the product biliverdin isomer distribution, since the in-plane seating preferences are different for the physiologically relevant aquo and spectroscopically convenient cyano complexes.

The very substantial perturbation of the axial His imidazole plane orientation relative to the protein matrix in the TM-hHO mutant relative to the WT has a reasonable rationalization. Crystal structures show (*14*, *15*) that the axial His25 imidazole $N_\delta H$ in WT-hHO serves as a donor to the side chain carboxylate of Glu29. The E29K mutation in TM-hHO abolishes this interaction with the imidazole ring, and some His ring rotational accommodation should not be unexpected. While the key proximal helix carboxylate side chain that is the link to the axial His ring $N_\delta H$ has not been mutated in other studies directed at modulating stereoselectivity (*25*, *26*, *30*, *32*), changes in axial His imidazole planes cannot be discounted. In hHO (*14*, *15*) and *C. diphtheriae* HO (*18*), the Glu linked to the axial His $N_\delta H$ also makes a strong contact to the methyl (or vinyl) at position e in Figure 2. In mutants that induce the 90° in-plane rotation of the substrate that accounts for *δ-meso* selectivity, a propionate replaces the methyl (or vinyl) at position e. It would be surprising if this altered contact with the Glu would not perturb its link to the axial His and hence the His ring orientation. Whether this perturbation due to the introduction of the propionate at position e is significant relevant to the determination of the substrate orientation can be readily addressed by assigning[4] the His $C_\beta H$'s in the mutants. The axial His imidazole plane orientation is likely more open to modulation by environmental factors (*51*) than is safe to assume for the simple use of Figure 4 to determine the substrate orientation.

ACKNOWLEDGMENT

We are indebted to Drs. N. Shokhirev and F. A. Walker for making available the Shift Pattern program.

SUPPORTING INFORMATION AVAILABLE

One table (chemical shifts for residues) and four figures (two NOESY spectra for TM-hHO−DMDH−CN, ratio of Ala28 NOEs to substrate methyls, NOESY contacts for His25 in hHO−PH−CN). This material is available free of charge via the Internet at http://pubs.acs.org.

REFERENCES

1. Tenhunen, R., Marver, H. S., and Schmid, R. (1969) Microsomal heme oxygenase. Characterization of the enzyme, *J. Biol. Chem. 244*, 6388−6394.
2. Ortiz de Montellano, P. R., and Auclair, K. (2003) Heme oxygenase structure and mechanism, in *The Porphryin Handbook* (Kadish, K. M., Smith, K. M., and Guilard, R., Eds.) pp 175−202, Elsevier Science, San Diego, CA.

3. Stocker, R., Yamamoto, Y., McDonagh, A. F., Glazer, A. N., and Ames, B. N. (1987) Biliruben is an antioxidant of possible physiological importance, *Science 235*, 1043−1046.
4. Baranano, D. E., and Snyder, S. H. (2001) Neural roles for heme oxygenase: Contrasts to nitric oxide synthase, *Proc. Natl. Acad. Sci. U.S.A. 98*, 10996−11002.
5. Uzel, C., and Conrad, M. E. (1998) Absorption of heme iron, *Semin. Hematol. 35*, 27−34.
6. Beale, S. I. (1994) Biosynthesis of open-chain tetrapyrroles in plants, algae, and cyanobacteria, *Ciba Found. Symp. 180*, 156−168.
7. Wilks, A. (2002) Heme oxygenase: Evolution, structure, and mechanism, *Antioxid. Redox Signaling 4*, 603−614.
8. Frankenberg-Dinkel, N. (2004) Bacterial heme oxygenases, *Antoxid. Redox Signaling 6*, 825−834.
9. Yoshida, T., and Migita, C. T. (2000) Mechanism of heme degradation by heme oxygenase, *J. Inorg. Biochem. 82*, 33−41.
10. Unno, M., Matsui, T., and Ikeda-Saito, M. (2007) Structure and catalytic mechanism of heme oxygenase, *Nat. Prod. Rep. 24*, 553−570.
11. Wenming, Z., Wilks, A., and Stojiljkovic, I. (2000) Degradation of heme in gram-negative bacteria: the product of the hemO gene of Neisseriae is a heme oxygenase, *J. Bacteriol. 182*, 6394−6403.
12. Wilks, A., and Schmitt, M. P. (1998) Expression and characterization of a heme oxygenase (HmuO) from Corynebacterium diphtheriae, *J. Biol. Chem. 273*, 837−841.
13. Caignan, G. A., Deshmukh, R., Wilks, A., Zeng, Y., Huang, H.-w., Moenne-Loccoz, P., Bunce, R. A., Eastman, M. A., and Rivera, M. (2002) Oxidation of heme to *β*- and *δ*-biliverdin by *Pseudomonas aeruginosa* heme oxygenase as a consequence of an unusual seating of the heme, *J. Am. Chem. Soc. 124*, 14879−14892.
14. Schuller, D. J., Wilks, A., Ortiz, de Montellano, P. R., and Poulos, T. L. (1999) Crystal structure of human heme oxygenase-1, *Nat. Struct. Biol. 6*, 860−867.
15. Lad, L., Wang, J., Li, H., Friedman, J., Bhaskar, B., Ortiz, de Montellano, P. R., and Poulos, T. L. (2003) Crystal structures of the ferric, ferrous and ferrous-NO forms of the Asp140Ala mutant of human heme oxygenase-1: Catalytic implications, *J. Mol. Biol. 330*, 527−538.
16. Sugishima, M., Sakamoto, H., Noguchi, M., and Fukuyama, K. (2003) Crystal structures of CO-, CN-, and NO-bound forms of rat heme oxygenase-1 (HO-1) in complex with heme: Structural implications for discrimination between CO and O2 in HO-1, *Biochemistry 42*, 9898−9905.
17. Friedman, J. M., Lad, L., Deshmukh, R., Li, H. Y., Wilks, A., and Poulos, T. L. (2003) Crystal structures of the NO- and CO-bound heme oxygenase from Neisseriae meningitidis—Implications for O2 activation, *J. Biol. Chem. 278*, 34654−34659.
18. Unno, M., Matsui, T., Chu, G. C., Coutoure, M., Yoshida, T., Rousseau, D. L., Olson, J. S., and Ikeda-Saito, M. (2004) Crystal structure of the dioxygen-bound heme oxygenase from *Corynebacterium diphtheriae*, *J. Biol. Chem. 279*, 21055−21061.
19. Sugishima, M., Migita, C. T., Zhang, X., Yoshida, T., and Fukuyama, K. (2004) Crystal structure of heme oxygenase-1 from cyanobacterium *Synechocystis* sp. PCC 6803 in complex with heme, *Eur. J. Biochem. 271*, 4517−4525.
20. Friedman, J., Lad, L., Li, H., Wilks, A., and Poulos, T. L. (2004) Structural basis for novel *δ*-regioselective heme oxygenation in the opportunistic pathogen *Pseudomonas aeruginosa*, *Biochemistry 43*, 5239−5245.
21. Frydman, R. B., Tomaro, M. L., Buldain, G., Awruch, J., Diaz, L., and Frydman, B. (1981) Specificity of heme oxygenase: A study with synthetic hemins, *Biochemistry 20*, 5177−5182.
22. Tomaro, M. L., Frydman, S. B., Frydman, B., Pandey, R. K., and Smith, K. M. (1984) The oxidation of hemins by microsomal heme oxygenase: Structural requirements for the retention of substrate activity, *Biochim. Biophys. Acta 791*, 342−349.
23. Gorst, C. M., Wilks, A., Yeh, D. C., Ortiz, de Montellano, P. R., and La, Mar, G. N. (1998) Solution ^{1}H NMR investigation of the molecular and electronic structure of the active site of substrate-bound human heme oxygenase: the nature of the distal hydrogen bond donor to bound ligands, *J. Am. Chem. Soc. 120*, 8875−8884.
24. La, Mar, G. N., Asokan, A., Espiritu, B., Yeh, D. C., Auclair, K., and Ortiz, de Montellano, P. R. (2001) Solution 1H NMR of the active site of substrate-bound, cyanide-ligated, human heme oxygenase. Comparison to the crystal structure of the water-ligated form, *J. Biol. Chem. 276*, 15676−15687.
25. Fujii, H., Zhang, X., and Yoshida, T. (2004) Essential amino acid residues controlling the unique regioselectivity of heme oxygenase in *Pseudomonas aeruginosa*, *J. Am. Chem. Soc. 126*, 4466−4467.
26. Deshmukh, R., Zeng, Y., Furci, L. M., Huang, H.-w., Morgan, B. N., Sander, S., Alontaga, A. Y., Bunce, R. A., Moenne-Loccoz, P., Rivera, M., and Wilks, A. (2005) Heme oxidation in a chimeric protein of the α-selective *Neisseriae meningitidis* heme oxygenase with the distal helix of the *δ*-selective *Pseudomonas aeruginosa*, *Biochemistry 44*, 13713−13723.
27. Wang, J., Evans, J. P., Ogura, H., La, Mar, G. N., and Ortiz, de Montellano, P. R. (2006) Alteration of the regiospecificity of human heme oxygenase-1 by unseating of the heme but not disruption of the distal hydrogen bonding network, *Biochemistry 45*, 61−73.
28. Hernández, G., Wilks, A., Paolesse, R., Smith, K. M., Ortiz, de Montellano, P. R., and La, Mar, G. N. (1994) Proton NMR investigation of substrate-bound heme oxygenase: Evidence for electronic and steric contributions to stereoselective heme cleavage, *Biochemistry 33*, 6631−6641.
29. Li, Y., Syvitski, R. T., Chu, G. C., Ikeda-Saito, M., and La, Mar, G. N. (2003) Solution ^{1}H NMR investigation of the active site molecular and electronic structures of the substrate-bound, cyanide-inhibited bacterial heme oxygenase from *C. diphtheriae*, *J. Biol. Chem. 279*, 6651−6663.
30. Zhou, H., Migita, C. T., Sato, M., Sun, D., Zhang, X., Ikeda-Saito, M., Fujii, H., and Yoshida, T. (2000) Participation of the carboxylate amino acid side chain in regiospecific oxidation of heme by heme oxygenase, *J. Am. Chem. Soc. 122*, 8311−8312.
31. Liu, Y., Zhang, X., Yoshida, T., and La, Mar, G. N. (2004) 1H NMR characterization of the solution active site structure of substrate-bound, cyanide-inhibited heme oxygenase from Neisseria meningitidis; Comparison to crystal structures, *Biochemistry 43*, 10112−10126.
32. Zeng, Y., Deshmukh, R., Caignan, G. A., Bunce, R. A., Rivera, M., and Wilks, A. (2004) Mixed regioselectivity in the Arg-177 mutants of *Corynebacterium diphtheriae* heme oxygenase as a consequence of in-plane heme disorder, *Biochemistry 43*, 5222−5238.
33. La Mar, G. N., Satterlee, J. D., and de Ropp, J. S. (2000) NMR of hemoproteins, in *The Porphyrins Handbook* (Kadish, K. M., Smith, K. M., and Guilard, R., Eds.) pp 185−298, Academic Press, San Diego, CA.
34. Li, Y., Syvitski, R. T., Auclair, K., Ortiz, de Montellano, P. R., and La, Mar, G. N. (2003) Solution ^{1}H, ^{15}N NMR spectroscopic characterization of substrate-bound cyanide-inhibited, human heme oxygenase: water occupation of the distal cavity, *J. Am. Chem. Soc. 125*, 13392−13403.
35. Shokhirev, N. V., and Walker, F. A. (1998) The effect of axial ligand plane orientation on the contact and pseudocontact shifts of low-spin ferriheme proteins, *J. Biol. Inorg. Chem. 3*, 581−594.
36. Shokhirev, N. V., and Walker, F. A. (1998) Co- and counterrotation of magnetic axes and axial ligands in low-spin ferriheme systems, *J. Am. Chem. Soc. 120*, 981−90.
37. Bertini, I., Luchinat, C., Parigi, G., and Walker, F. A. (1999) Heme methyl 1H chemical shifts as structural parameters in some low-spin ferrheme proteins, *J. Biol. Inorg. Chem. 4*, 515−519.
38. Rivera, M., and Caignan, G. A. (2004) Recent developments in the ^{13}C NMR spectroscopic analysis of paramagnetic hemes and heme proteins, *Anal. Bioanal. Chem. 378*, 1464−1483.
39. Li, Y., Syvitski, R. T., Auclair, K., Wilks, A., Ortiz, de Montellano, P. R., and La, Mar, G. N. (2002) Solution NMR characterization of an unusual distal H-bond network in the active site of the cyanide-inhibited, human heme oxygenase complex of the symmetric substrate, 2,4-dimethyldeuterohemin., *J. Biol. Chem. 277*, 33018−33031.
40. Jeener, J., Meier, B. H., Bachmann, P., and Ernst, R. R. (1979) Investigation of exchange processes by two dimensional NMR spectroscopy, *J. Chem. Phys. 71*, 4546−4553.
41. Neuhaus, D., and Williamson, M. (2000) *The Nuclear Overhauser Effect in Structural and Conformational Analysis*, 2nd ed., Wiley-VCH Publishers, New York.
42. Bonnett, R., and McDonaugh, A. F. (1973) The meso-reactivity of porphyrins and related compounds. VI. Oxidative cleavageof the haem system. The four isomeric biliverdins of the IX series., *J. Chem. Soc., Perkin Trans. 1 1*, 881−888.

43. Sandström, J. (1982) *Dynamic NMR Spectroscopy*, Academic Press, New York.
44. Wüthrich, K. (1986) *NMR of Proteins and Nucleic Acids*, Wiley & Sons, New York.
45. Bertini, I., and Luchinat, C. (1996) NMR of paramagnetic substances, *Coord. Chem. Rev. 150*, 1−296.
46. La, Mar, G. N., Kolczak, U., Tran, A.-T., and Chien, E. (2001) Solution ^{1}H NMR characterization of axial interactions of the proximal and distal His in the cyanomet complexes of the isolated chains and 65 kDa intact tetramer of human hemoglobin, *J. Am. Chem. Soc. 123*, 4266−4274.
47. Hauksson, J. B., La, Mar, G. N., Pandey, R. K., Rezzano, I. N., and Smith, K. M. (1990) NMR study of heme pocket polarity/hydrophobicity of myoglobin using polypropionate-substituted hemins, *J. Am. Chem. Soc. 112*, 8315−8323.
48. La, Mar, G. N., Hauksson, J. B., Dugad, L. B., Liddell, P. A., Venkataramana, N., and Smith, K. M. (1991) Proton NMR study of the heme rotational mobility in myoglobin: The role of propionate salt-bridges in anchoring the heme, *J. Am. Chem. Soc. 113*, 1544−1550.
49. Tran, A.-T., Kalish, H., Balch, A. L., and La Mar, G. N. (2000) Solution 1H NMR investigation of the seating and rotational "hopping" of centro-symmetric etioheme-I in myoglobin. Effect of globin roigin and its oxidation spin state on heme dynamics, *J. Biol. Inorg. Chem. 5*, 624−633.
50. Zhu, W., Li, Y., Wang, J., Ortiz, de Montellano, P. R., and La Mar, G. N. (2006) Solution NMR study of environmental effects on substrate seating in human heme oxygenase; Influence of polypeptide truncation, substrate modification and axial ligand, *J. Inorg. Biochem. 100*, 97−107.
51. Liu, Y., Ma, L.-H., Zhang, X., Yoshida, T., Satterlee, J. D., and La Mar, G. N. (2006) ^{1}H NMR study of the influence of hemin vinyl-methyl substitution on the interaction between the C-terminus and substrate and the "aging" of the heme oxygenase from *N. meningitidis*. Induction of active site structural heterogeneity by a two-fold symmetric hemin, *Biochemistry 45*, 13875−13888.

BI7017333